Tenth International Conference on Computational Fluid Dynamics (ICCFD10), Barcelona, Spain, July 9-13, 2018 **ICCFD10-0297**

Investigation into Wake Integration Technique for Airplane Drag Prediction

K. Matsushima*, R. Shimizu* and Y. Takahashi*
Corresponding author: kisam@eng.u-toyama.ac.jp

* Dept. Mechanical Engineering, University of Toyama, Japan

Abstract: The article performed drag calculations using four wake integration equations. First one came from the equation of momentum conservation law itself, second one was based on enthalpy variation, third is based on entropy variation and the last one was a method for induced drag calculation. The drag calculation was applied CFD simulation results in order to utilize wake flow information as well as to devise strategies for predicting accurate drag values. Through the investigation of wake integration drag values, we found the role of enthalpy variation and several pieces of interesting knowledge.

Keywords: Aircraft wakes, CFD, Drag, Far-field integration, Total enthalpy production.

1 Introduction

For aerodynamic design of airplanes, it is important to obtain accurate drag prediction tools. There have been two ways of calculating drag force on an airplane. One is by integrating pressure and skin-friction acting on the airplane surface, which is called "near-field" calculation. The other is by integrating the deficits of momentum flux and pressure over the surfaces of a control volume surrounding the airplane in a flow-field, which is "far-field" calculation. Moreover, it has been found that the integration domain can be reduced to only a downstream (outflow) surface. The integration results on the other surfaces should be negligible when the control volume is appropriately selected. The reduced form of "far-field" calculation is called "wake integration" method. The method was firstly developed for wind tunnel experiment by Betz in the early twenties century. Then, the method has been improved and extended to meet the need for accurate lift and drag prediction in wind tunnel experiment [1]. In the field of CFD, "near-field" calculation is popular to obtain drag forces. But alternative method is welcome to obtain more reliable drag values. Several research groups have been actively involved in "wake integration" for both experiment and CFD drag prediction [2-4]. In the article, we investigate resulted drag values by using several kinds of wake integration equations. The "wake integration" is conducted on flow-fields by RANS CFD simulation. The drag values are compared with "near-field" one. The effect of a wake plane position along freestream direction (*x*-axis) on predicted drag values is examined. In addition, we discuss the interesting behavior of a spurious total enthalpy increase (ΔH) by CFD computation. Then, the role of the spurious ΔH is considered in "wake integration".

2 Basic Equations of Wake Integration for Drag Prediction

2.1 Near-field Method

Drag by the "near-field" method $D_{surface}$, is calculated using the following equation;.

$$D_{surface} = \iint_{S_0} [\, P \cdot n_x - \vec{\tau}_x \cdot \vec{n}\,]\, dS \tag{1}$$

where P is pressure, $\vec{n}$ is a unit normal vector and $\vec{\tau}_x$ indicates the x-directional component $(\tau_{xx}, \tau_{yx}, \tau_{zx})$ of a viscous stress tensor on the airplane (wing) surface S_0 in Figs. 1 and 2.

2.2 Wake Integration Method

Several kinds of wake integration are used to predict a drag value in this article. The first one is the primary equation of Eq. (2) which is directly derived from the integral form of momentum conservation law (*i.e.* Navier-Stokes equations).

$$D \;\; = \iint_{S_2} [\, \rho u \,(U_\infty - u) + (P_\infty - P)]\, dS \tag{2}$$

The second, third and fourth ones are expressed in the following equations derived from the perturbation form of Eq. (2). They are derived in order to decompose drag D into several elements which are enthalpy drag D_h, profile drag (entropy drag) D_p and induced drag D_i [1].

$$D_h = \iint_{S_2} \rho_\infty \Delta H \; dS \tag{3}$$

$$D_p = \iint_{S_2} P_\infty \frac{\Delta s}{R} dS - \iint_{S_2} \frac{P_\infty}{2} \left(\frac{\Delta s}{R}\right)^2 dS \tag{4}$$

$$D_i = \iint_{S_2} \frac{\rho_\infty}{2} (v^2 + w^2) dS - \iint_{S_2} \frac{\rho_\infty}{2} \left(1 - {M_\infty}^2\right) (\Delta u)^2 dS \tag{5}$$

Some symbols used in Eqs. (1) - (4) are illustrated in Fig. 1 and 2. S_2 plane is perpendicular to freestream (U_∞) direction. Here, U_∞ direction is along the x-axis. D represents total drag Eq. (2) is the basic form of the momentum balance theorem. ρu is x-momentum and P is pressure. $\Delta H = H - H_\infty$ where H is total enthalpy. D_p is the drag due to entropy generation ($\Delta s = s - s_\infty$). D_i is related to lift. (u, v, w) is a velocity vector in the rectangular coordinate (x, y, z). M_∞ indicates the freestream Mach number of a flow-field.

From an theoretical point of view, $D_{surface} \cong D \;\; \cong D_h + D_p + D_i$. If an airplane has no powered engine, ΔH is negligible so that D_h yeilds to zero. On the other hand, we have found that CFD computation produces spurious ΔH if there is no powered engine through research on the wake integration. The target flow-fields for wake integration are those around a wing and a wing and fuselage combination, shown in later. There is no engine, but wake integration over CFD results gives substantial amount of enthalpy drag. That is why D_h is mentioned here..

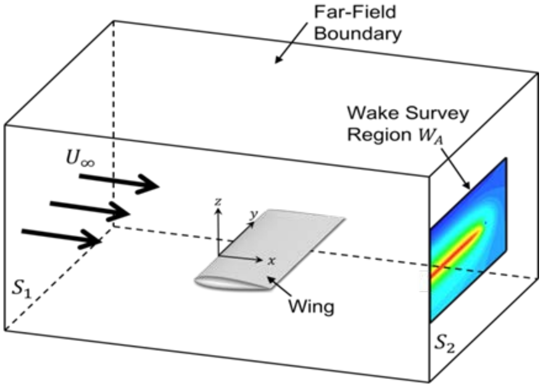

Figure 1: A wing, a flow-field and wake.

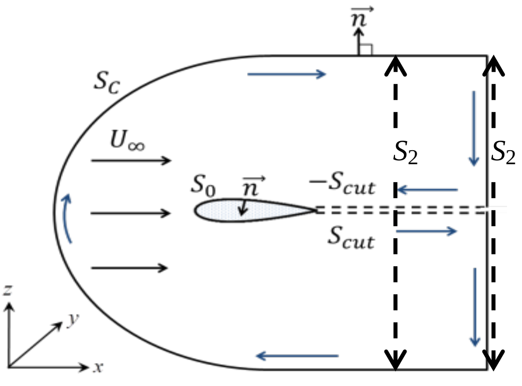

Figure 2: 2D sketch of wake integration path.

3 Flow-field for Drag Prediction

For the drag prediction, two examples of flow-fields are prepared. Both were RANS (Reynolds Averaged Navier -Stokes) simulation results. One is flow about a NASA CRM wing-fuselage model (Fig. 3) [5,6]; the flow speed is Mach 0.85, the angle of attack (AOA) is 4.84° and Reynolds number is 2.26 million. We simulate the left side of the flow-field using symmetrical conditions. The far-field boundary location is 50 times of MAC length away from the airplane body. MAC length means the mean average chord length of a wing. Then, the size of computational domain in each of *x*, *y*, *z* direction is from -50C to 50C, from 0 to 50C and, -50C to 50C, respectively. C means MAC length. The Mesh around the CRM is unstructured and the total number of mesh points is about 26million. Eight locations along the *x* coordinate are selected to perform wake integration for drag as shown in Fig. 4. The other is that past a rectangular wing (Fig. 5) whose section shape is NACA0012; the speed is Mach 0.82, AOA is 4.84° and Reynolds No. is 3.0 million. Concerning the computational space for the simulation, the CRM model case is sufficiently large. Conversely, that for wing simulation case is small. We performed the flow simulation around the rectangular wing with two different computational spaces. The far-field boundary location of the first one is ten times of MAC length away from the wing, and the other is twenty times of MAC length away. Then, the size of computational domain for the first wing case in each of *x*, *y*, *z* direction is from -10C to 11C, from 0 to 15C and, -10C to 10C, respectively. That for the second wing case is from -20C to 21C in *x*, from 0 to 30C in *y* and, -20C to 20C in *z*. The total number of mesh points for each case is 1.16 million and 1.53 million, respectively.

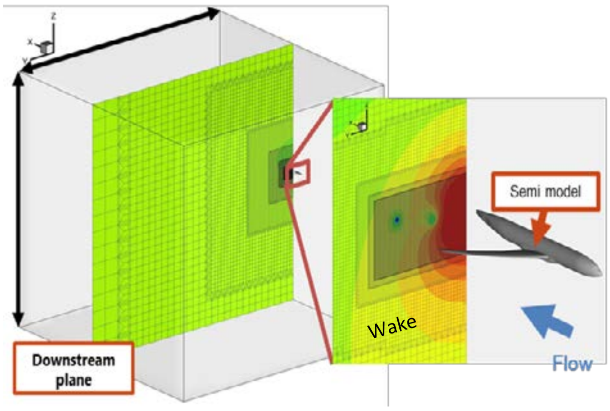

Figure 3: Flow-field and mesh about a CRM wing-fuselage model.

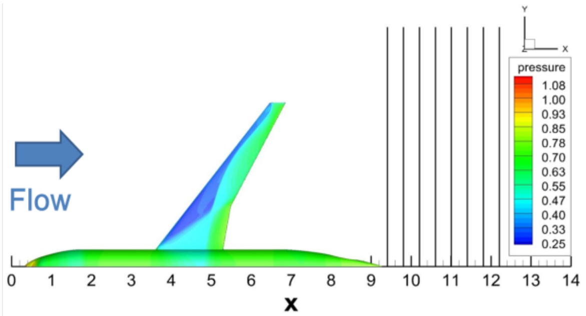

Figure 4: Location of wake planes downstream from the CRM model end.

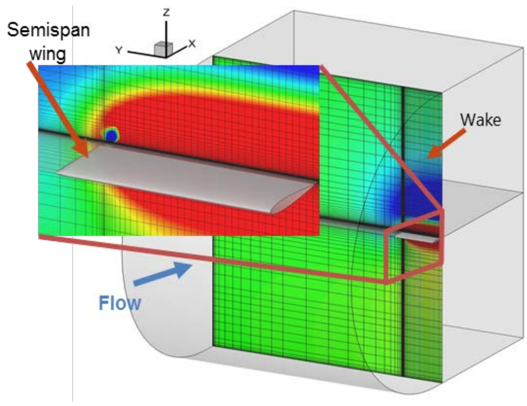

Figure 5: Flow-field and mesh about a rectangular wing model.

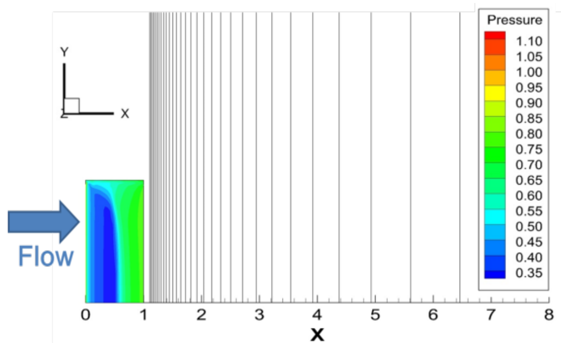

Figure 6: Location of wake planes downstream from the wing trailing edge.

The treatment of the far-field boundary affects the quality of drag values by wake integration [7]. As readers will see in the next section, if the far-field boundary location of a computational domain is not sufficiently far away, non-physical spurious enthalpy production takes place in RANS simulation.

4 Discussion on Wake Integration on CRM Simulation

From here, drag values are transformed to drag coefficients, such that D is transformed to CD and D_h is to CD_h while "near-field drag is to $CD_{surface}$. The integral area of a wake plane S_2 is selected as a square whose edges range from -20C to 20C in the z direction and from 0 (the symmetrical center line position) to 20C in the y direction at each x location.

4.1 Drag from Momentum Balance Equation and Enthalpy Drag

Figure 7 shows CD and CD_h dependency on the wake plane position along the x-axis of the CRM model. The rear end of the airplane is at the x of 9.3C. For the model, the computational space was large enough. CFD calculation does not produce spurious enthalpy variation. Therefore, CD_h (red circles) is zero. On the every wake plane in Fig. 7, the CD derived from the momentum balance equation gives proper values almost same as $CD_{surface}$. There is little dependency on the x location of wake plane, S_2. The quantity of each drag coefficient by wake integration on the plane of x=11 is also listed in a table format in Fig. 7.

4.2 Profile Drag and Induced Drag

Figure 8 compares CDp, CDi, the sum of CDp and CDi which is denoted by CDt and $CD_{surface}$ at eight different location of a wake plane, S_2. As expected, CDt agrees very well. The CDt value does not depend on the x location of a wake plane. Accurate drag prediction can be also performed by calculating CDp and CDi. Induces drag shares about thirty percent of total drag, which is a proper percentage [8, 9]. Then, we think Eq. (4) and Eq. (5) works well. The decomposition of total drag into drag elements, such as profile and induced drags, is to be successfully performed using those equations. The drag decomposition is very useful for aerodynamic design of aircraft. Precise analysis on quantitative difference among drag predictions by near-field and wake integration methods should be done in the future.

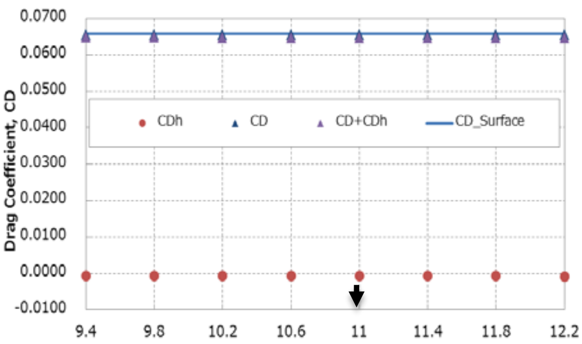

CD_h	−0.0006804
CD	0.0655573
$CD+CD_h$	0.0648769
$CD\_{surface}$	0.0658952

Figure 7: CD by Eq.(2) and CD_h by Eq.(3) compared with Near-field $CD_{surface}$. Their values at the wake plane, x=11C.

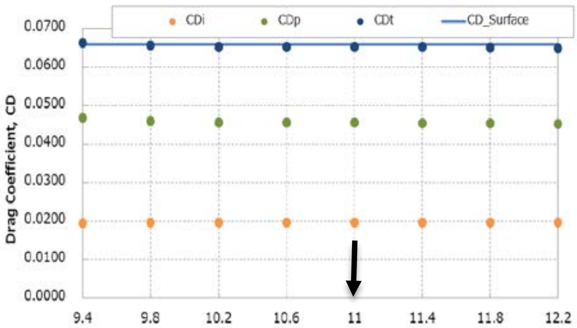

CDp	0.045552
CDi	0.019681
$CDt=CDi+CDp$	0.065233
$CD\_{surface}$	0.065895

Figure 8: CD_p by Eq.(3) and CD_i by Eq.(4) compared with Near-field $CD_{surface}$. Their values at the wake plane, x=11C.

5 Discussion on Wake Integration on Rectangular Wing Simulation

In this section and after, the first wing case of the smaller computational domain is identified as "FF10" and the other of the larger domain is identified as "FF20".

5.1 Drag from Momentum Balance Equation and Enthalpy Drag

CD, CD_h and the sum of those two drag coefficients by wake integration of the wing model flow-field are plotted in Figs. 9 and 10. The horizontal axis is the distance of a wake plane downstream from the wing leading edge. The distance of the trailing edge is 1.0. The vertical one indicates drag coefficient value. The near-field drag coefficient is also shown with a blue straight line. Figure 9 presents *CD* and CD_h on the wake plane position along the *x*-axis of "FF10" with the far-field boundary location of 10C, while Fig. 10 dose of "FF20" with the far-field boundary location of 20C. The quantity of each drag coefficient is also presented in Fig, 9 and 10. For the wing case, *CD* values are much less than CD_{surface}. *CD* increases as the size of the computational domain becomes larger. It decreases as the wake plane location moves further downstream from the wing trailing edge. The enthalpy drag coefficient CD_h cannot be neglected. Moreover, its behavior is very interesting. In fact, it compensates for the difference of *CD* from $CD_{surface}$ on every wake plane at a different *x* position in Figs 9 and 10. In FF10 and FF20 graphs, the sum of *CD* and CD_h is almost same as $CD_{surface}$. The error is less than 0.1 percent. There is little dependency of the value of $CD + CD_h$ on the position of a wake plane.

Since we encounter the interesting behavior of CD_h, the contour map of the integrant of Eq. (3), $\rho\Delta H$ is visualized in the whole computational domain. Figure 11 shows the distribution of $\rho\Delta H$ on the *x*-*z* plane at y=0 (symmetrical center plane) of "FF10". There can be recognized a certain amount of $\rho\Delta H$ in the substantially wide region near the far-field boundary. Figure 12 shows the distribution of "FF20". In Fig. 12, the distribution looks much more natural than that in Fig. 11, because there is no total enthalpy variation in the region except the area of a wing, its boundary layers and wakes. However, even the case of "FF20", CD_h is not negligible at all and a certain amount of $\rho\Delta H$ still remains near the far-field boundaries. The whole domain of "FF10" in Fig.11 corresponds to the subdomain inside a closed curve of blue dotted lines in Fig. 12. Their flow physics in terms of total enthalpy is totally different from each other though they are geographically same. So, inappropriate location of far-field boundary and imposing free stream flow variables at the far-field boundaries cause total enthalpy variation. Through the observation of Figs. 11 and 12, we understand that this total enthalpy variation near far-field boundaries should not be real physics, it is spurious. We also think the spurious enthalpy could be useful for evaluating the quality of mesh and far-field boundary conditions imposed in CFD simulation..

5.2 Profile Drag and Induced Drag

Figure 12 shows *CDp*, *CDi*, the sum of *CDp* and *CDi* which is denoted by *CDt* compared with near field drag coefficient $CD_{surface}$. Those *CD* values are obtained from "FF10". The horizontal axis is the distance of a wake plane downstream from the wing leading edge. The distance of the trailing edge is 1.0. The vertical one indicates drag coefficient value. In the vicinity of the wing trailing edge, each *CD* value changes rapidly with the distance increase. After it reaches 2.5, all the *CD* vales keep constant. *CDt* agrees $CD_{surface}$ in less than one present error. It looks like that drag decomposition works successfully. The induced drag rate in the total drag is about fifteen percent. The rate is less than that of CRM model in the section 4. It is because strong shock waves are generated in wing simulation. Shock waves cause additional profile drag. Thus, the induced drag rate becomes relatively lower than a weak shock wave case on swept wing.

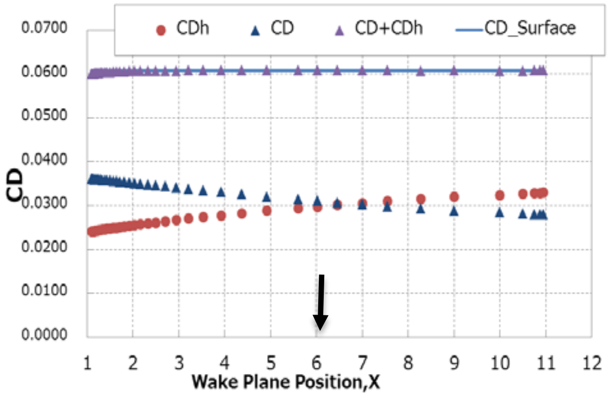

CD_h	0.029685
CD	0.031115
$CD+CD_h$	0.060800
$CD_{Surface}$	0.060838

Figure 9: CD by Eq.(2) and CD_h by Eq.(3) compared with Near-field $CD_{surface}$ of FF10. Their values at the wake plane, $x≒6.0$.

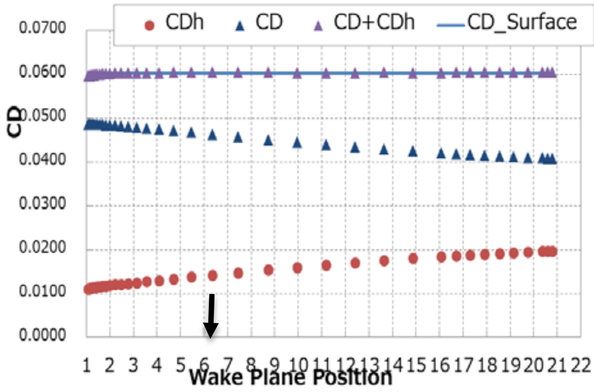

CDh	0.014123
CD	0.046277
$CD+CDh$	0.060400
$CD_{Surface}$	0.060340

Figure 10: CD by Eq.(2) and CD_h by Eq.(3) compared with Near-field $CD_{surface}$ of FF20. Their values at the wake plane, $x≒6.0$.

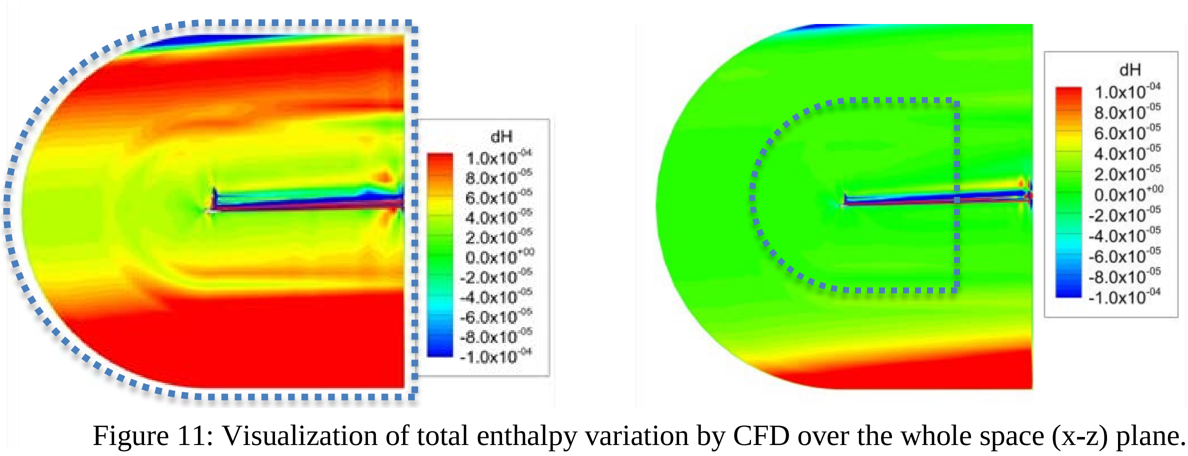

Figure 11: Visualization of total enthalpy variation by CFD over the whole space (x-z) plane. Left: FF10 (the smaller domain), Right: FF20 (the larger domain) .

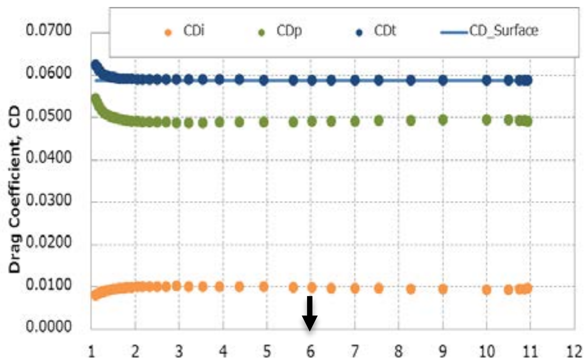

CDp	0.049885
CDi	0.010592
$CDt=CDi+CDp$	0.060377
$CD_{surface}$	0.060834

Figure 12: CD_p by Eq.(3) and CD_i by Eq.(4) compared with Near-field $CD_{surface}$. Their values at the wake plane, $x≒6.0$.

6 Conclusions and Future Work

Drag calculations were conducted for CFD simulation results to examine the performance of wake integration. Four wake integration equations were used. First one (D) came from the equation of momentum conservation law itself, second one (D_h) was based on enthalpy variation, third (D_p) is based on entropy variation and the last one (Di) was for induced drag calculation. They were applied to several kinds of flow-fields by CFD simulation around a NASA CRM wing-fuselage configuration and a rectangular wing. Drag values by wake integration were compared with "near-field" drag ($D_{surface}$). First, we found an interesting behavior of D_h. Theoretically, D_h should be zero, but it had a substantial value when a computational domain for CFD simulation was not large enough. Then, the spurious D_h seemed to compensate D calculation. In other word, the equation of $D+ D_h = D_{surface}$ was valid for every CFD simulation. Secondly, drag decomposition was successfully done into D_p, profile drag and Di, induced drag. Then, the equation of $D+ D_h = D_{surface}$ was also confirmed. Thus, the error among several kinds of wake integration and near-field drag was less than one percent through the examination. At last, total drag using wake integration equations was little dependency on the wake plane position. However, a wake plane located less than 1.5 times of MAC length behind an airplane body end was inappropriate. Precise quantitative analysis of drag predictions by near-field and wake integration methods should be done in the future

Acknowledgment

This work was supported by JSPS KAKENHI Grant Number JP16K06884. I appreciate their support.

References

[1] K. Kusunose ; *A Wake Integration Method for Airplane Drag Prediction*, Tohoku University Press, ISBN4-86163-015-0 C3353, March 2005.

[2] M. Meheut and D. Baily ; Drag-Breakdown Methods from Wake Measurements, *AIAA J*., 46(4):847-862, April 2008.

[3] B. Mele, M. Ostieri, and R. Tognaccini ; Aircraft Lift and Drag Decomposition in Transonic Flows, *Journal of Aircraft*, 54(5):1933-1944, Oct, 2017.

[4] W. Yamazaki, K. Matsushima, K. Nakahashi ; Drag prediction, decomposition and visualization in unstructured mesh CFD solver of TAS-code, International Journal for Numerical Methods in Fluids, Vol. 57, Issue 4, pp.416-436, 2008.

[5] https://cfdws.chofu.jaxa.jp/apc/

[6] A. Hashimoto et. al. ; Summary of First Aerodynamics Prediction Challenge (APC-I), AIAA Paper 2016-1780, 54th AIAA Aerospace Sciences Meeting, Jan. 2016.

[7] R. Shimizu, K. Matsushima and K. Goshima ; Investigation on numerical drag prediction for airplanes by wake integration, *JAXA-SP-17-004*, ISSN 1349-113X:127-132, Dec. 2017 (in Japanese).

[8] D. L. Hunt and M. B. Giles ; Wake Integration for Three-Dimensional Flow-field Computations: Applications, Journal of Aircraft, Vol. 36, No. 2, pp. 366-373, April, 1999.

[9] M. Ueno, K. Yamamoto, K. Tanaka, M. Murayama ; Far-Field Drag Analysis of NASA Common Research Model Simulation, Journal of Aircraft, 50(2), 388-397, April 2013.